



# On the Effectiveness of the Iterative Coupling FEM–BEM for the Analysis of the Problems with Elastoplastic Failure Behavior

Daho Boumaiza · Benaoumeur Aour

Submitted: 20 February 2022 / Accepted: 17 March 2022 / Published online: 18 April 2022  
© ASM International 2022

**Abstract** The main purpose of this paper is to investigate the interface relaxation FEM–BEM coupling method to resolve problems involving nonlinear fracture mechanics. In this coupling technique, the nonlinear portion near the crack tip is modeled by the finite element method (FEM) and the remainder of the domain which is linear elastic is discretized using the boundary element method (BEM). In the coupling procedure adopted here, there is no need to combine the coefficients matrices of FEM and BEM subdomains and separate computing for each subdomain with successive renewal of the variables on the interface are performed to reach the final convergence. To demonstrate the effectiveness of the developed approach, several practical problems of nonlinear fracture mechanics are analyzed. The conventional FEM computations are also performed, and a critical comparison of the results is made.

**Keywords** Iterative coupling FEM–BEM · FEM · BEM · Elastoplastic fracture mechanics

## Abbreviations

**a** Crack length  
**b** Vector of distributed load/unit volume  
**B** Elastic strain displacement matrix

---

D. Boumaiza · B. Aour (✉)  
Laboratory of Applied Biomechanics and Biomaterials (LABAB), ENP Oran, BP 1523, 31000 El Mnaouer, Oran, Algeria  
e-mail: ben\_aour@yahoo.fr

D. Boumaiza  
Faculty of Science and Technology, University Mustapha Stambouli of Mascara, Route de Mamounia Mascara, BP 305, Mascara 29000, Algeria

$c_{ij}$  Tensor dependent on the location of the field point  
 $D_{ep}$  Tangential elastoplastic modular matrix  
 $E$  Elasticity modulus for plane stress conditions  
 $E'$  Elasticity modulus for plane strain conditions  
 $\mathbf{f}$  External applied forces  
 $f$  Yield function  
 $\{\mathbf{F}_F^F\}$  Forces vector applied on the FEM subdomain  
 $\{\mathbf{F}_F^I\}$  Forces vector applied on the FEM/BEM interface  
 $\mathbf{G}, \mathbf{H}$  Influence coefficient matrices  
 $G$  Shear modulus of the material  
 $h$  Hardening parameter  
 $K_{I,II,III}$  Stress intensity factors in mode I, II and III.  
 $\mathbf{K}$  Stiffness matrix for the overall structure  
 $[\mathbf{K}^e]$  Elementary stiffness matrix  
 $M$  Number of boundary elements.  
 $\mathbf{N}$  Shape functions matrix  
 $r$  Distance between the field point and the source point  
 $p$  Internal point.  
 $\{\Delta \mathbf{p}\}$  Incremental elementary force vector  
 $\{\Delta \mathbf{R}\}$  Vector of the boundary values for the tractions  
 $\{\mathbf{t}\}$  Incremental force vector  
 $\{\mathbf{t}_B^B\}$  Tractions vector applied on the BEM subdomain  
 $\{\mathbf{t}_B^I\}$  Tractions vector applied on the FEM/BEM interface  
 $\mathbf{T}(p, Q)$  Matrix containing fundamental solution for the tractions at point  $p$   
 $\{\mathbf{u}\}$  Vector of the boundary values of the displacements  
 $\{\mathbf{u}_B\}$  Displacement vector of the BEM subdomain  
 $\{\mathbf{u}_B^I\}$  Displacement vector of the FEM/BEM interface

$\{\mathbf{u}_B^B\}$	Displacement vector of the BEM subdomain except $\{\mathbf{u}_B^I\}$
$\{\mathbf{u}_F\}$	Displacement vector of the FEM subdomain
$\{\mathbf{u}_F^I\}$	Displacement vector of the FEM/BEM interface
$\{\mathbf{u}_F^c\}$	Displacement vector of the FEM subdomain except $\{\mathbf{u}_F^I\}$
$\mathbf{U}(p, Q)$	Matrix containing fundamental solution for the displacements at point $p$
$U$	Strain energy density
$\{\Delta \mathbf{u}_n\}$	Incremental displacement vector at the nodes
$\{\Delta U\}^c$	Incremental strain energy in the element
$\mathbf{x}$	Vector containing coordinates
$\mathbf{x}_f$	Field point
$\mathbf{x}_s$	Source point
$\alpha$	Subtended angle from point $p$ to the boundary
$\delta_{ij}$	Kronecker delta symbol
$\{\Delta \Pi\}$	Incremental potential energy stored.
$\boldsymbol{\varepsilon}$	Strain vector
$\bar{\varepsilon}_p$	Effective plastic strain
$\{\Delta \boldsymbol{\varepsilon}\}^c$	Incremental strain vector of the element
$\Gamma$	Boundary of the domain $\Omega$
$\nu$	Poisson's ratio
$\boldsymbol{\sigma}$	Stress vector
$\bar{\sigma}$	Effective stress
$\sigma_Y$	Yield stress
$\{\Delta \boldsymbol{\sigma}\}^c$	Incremental stress vector of the element.
$\Omega$	Two-dimensional arbitrary domain
$\omega$	Relaxation parameter
$\xi$	Local coordinate
$\{\Delta \boldsymbol{\psi}\}$	Residual force vector
BB	Superscript indicating boundary element subdomain without interface
BE	Superscript indicating boundary element subdomain
FE	Superscript indicating finite element subdomain
FF	Superscript indicating finite element subdomain without interface
I	Superscript indicating interface FEM/BEM subdomains
IB	Superscript indicating interface boundary element subdomain
IF	Superscript indicating interface finite element subdomain

## Introduction

The finite element method (FEM) is a powerful and versatile approach for the solution of a wide class of practical problems. It is often the method of choice for solving

inhomogeneous, anisotropic, and nonlinear problems [1]. The boundary element method (BEM) is a good alternative approach, especially for elastic linear and isotropic problems with infinite extension and regions of high-stress concentration [2]. The main advantage of the BEM is that due to the modeling only of the boundary of the bodies, there is a reduction of the problem dimensionality by one, which results in significantly decreasing the modeling time. However, BEM is not preferable when there are inhomogeneities and non-linearities in the analysis domain. Thus, each method performs better than the other in some domains or some parts of the same domain. Therefore, a combined formulation that couples FEM and BEM and exploits the potential of each method seems to be very useful.

In the case of nonlinear fracture mechanics, the plastic region is restricted near the crack-tip and their main region can be treated as linear elastic. In such a problem, an intermarriage of FEM and BEM is conceptually and computationally very attractive. It permits to retain the advantages of each method since it allows discretization of only this limited plastic zone by finite elements, rather than that of the entire domain. The rest can be easily modeled using BEM in which nodal points are only needed on the boundary instead of throughout the region as required by the FEM.

From the historical point of view, it seems that the well-established first paper in this fruitful research area is that of Zienkiewicz et al. [3]. Then, a variety of combined approaches has been later developed by several authors [4–8]. An overview of the literature on this topic published before 2004 has been presented by Ganguly et al. [9]. The development and analysis of new techniques for coupling FEM–BEM have been the subject of growing interest in recent years. It has been investigated extensively and applied to different areas such as elastostatics [10–12], elastoplastic [6, 13], viscoelastic [14, 15], dynamics [8, 16], fracture mechanics [17–19], biomechanics [20], heat transfer [21, 22], contact [23, 24], fluid–structure interaction [25, 26], soil–structure interaction [27, 28], acoustics [29, 30], magnetostatic problems [31, 32], and isogeometric [33].

In general, the existing coupling approaches can be roughly classified into three main categories: (1) FE hosted, in which BEM subdomain is treated as a macro-finite element (i.e., in this case, the boundary element equations are transformed into an equivalent force-displacement equations system). (2) BE hosted in which, FE subdomain is treated as an equivalent BE subdomain (i.e., the FEM equations are transferred into traction-displacement equations system) and (3) FE–BE approach which gathers those, which are not included in either of the two above approaches.

The first two approaches of coupling (FE hosted and BE hosted) have been studied thoroughly in the literature [3–10, 34]. In fact, merging two different kinds of programs together to form an integrated finite element boundary element software environment will require considerable effort and has a negative effect on the strong points of each method. Hence, a change in strategy used in the coupling procedure was undertaken to overcome some difficulties and make the coupling method more efficient. In this context, the most appealing ones are those which preserve the features of each method. Among those appears the coupling method by an interface relaxation procedure which has been selected in this work to deal with elastoplastic fracture mechanics problems. The main advantage of this coupling technique that it does not need to modify the FEM or BEM matrices, but a separate computing will be carried out for each subdomain what allows the direct use of software packages.

The purpose of this paper is to extend the iterative coupling FEM–BEM approach for solving the nonlinear problems of elastoplastic fracture mechanics and to highlight its effectiveness by considering different behaviors, hardenings, loadings, and configurations. To achieve this objective, the paper is organized as follows. In the second section, the FEM–BEM discretization is presented. Noting that the linear elastic part is modeled by BEM, and however, the nonlinear elastoplastic subregion in the vicinity of the crack is modeled by FEM. Details about the application of both methods in such subregions are given in sections 3 and 4. The use of J-integral in elastoplastic fracture is described in section 5. The iterative FEM–BEM coupling and its implementation are outlined in section 6. Finally, the proposed coupling procedure is carried out for several practical examples to illustrate its applicability, its accuracy, and its efficiency for the analysis of the cracked structures.

### FEM–BEM Discretization

In this work, an interface relaxation FEM–BEM coupling method was developed. To carry out this approach, the original problem is decomposed into two subproblems as shown in Fig. 1. The first is related to an elastoplastic subdomain  $\Omega^{FE}$  containing cracks, while the other is a linear elastic subdomain  $\Omega^{BE}$ . The first is modeled by FEM and the second by BEM. The final solution is then obtained by combining the two subproblems at the common interface  $\Gamma^I = \Gamma^{IF} = \Gamma^{IB}$ . The remaining parts of the boundaries in the FEM and BEM subdomains are denoted by  $\Gamma^{FF}$  and  $\Gamma^{BB}$ , respectively.

It is important to note that this FEM–BEM coupling procedure yields a group of approximately independent

subproblems of lower computational difficulty [35]. This technique considers the separate analysis of the linear and nonlinear subproblems by preserving the advantages of both methods FEM and BEM.

It should be noted that to ensure a correct coupling between both methods, the conditions of equilibrium and compatibility must be satisfied. The meshes are compatible if both have common nodes at the interface and the degree of interpolation functions used in FEM and BEM is identical. Thus, we have used 8-noded isoparametric quadrilateral elements for the finite element subdomain, and 3-noded isoparametric quadratic elements in the boundary element formulation as shown in Fig. 1. In what follows, we perform the appropriate formulation for each subdomain, and then, we apply the iterative principle on the interface between both subdomains to carry out the coupling.

### Boundary Element Modeling of Elastic Subdomain

In this section, we will briefly introduce the applicability of the direct BEM for the analysis of the elastic linear subregion which will be coupled with the nonlinear finite element’s subregion. Indeed, the BEM has many positive attributes that make it advantageous for the use in the elastic linear region of cracked ductile structures. A widely recognized advantage of the BEM is that it reduces by one the dimensionality of the problem which leads to a reduced system of equations of freedom [2, 36]. This is particularly advantageous for numerical fracture mechanics because fewer degrees of freedom imply greater numerical stability in the solution process [37]. In this work, 3-noded isoparametric parabolic elements are used (Fig. 2). By using the matrix notation, the geometry of each boundary element and the variation of the displacement and traction can be expressed as function of the local coordinate,  $\xi$  as follows:

$$\begin{aligned} \mathbf{x}(\xi) &= \mathbf{N}(\xi) \mathbf{x}^e \\ \mathbf{u}(\xi) &= \mathbf{N}(\xi) \mathbf{u}^e \\ \mathbf{t}(\xi) &= \mathbf{N}(\xi) \mathbf{t}^e \end{aligned} \tag{Eq 1}$$

where  $\mathbf{x}$ ,  $\mathbf{u}(\xi)$  and  $\mathbf{t}(\xi)$  are, respectively, vectors containing coordinates, displacements and tractions components at  $\xi$ ;  $\mathbf{x}^e$ ,  $\mathbf{u}^e$  and  $\mathbf{t}^e$  are vectors of the corresponding values at the element nodes, and  $\mathbf{N}(\xi)$  is matrix containing the shape functions for 3-noded isoparametric quadratic elements, i.e.,:

$$\begin{aligned} N_1(\xi) &= \frac{1}{2}\xi(\xi - 1), & N_2(\xi) &= (1 - \xi^2), \\ N_3(\xi) &= \frac{1}{2}\xi(\xi + 1) \end{aligned} \tag{Eq 2}$$

In the direct formulation of the BEM, a numerical solution for a body of domain  $\Omega$  with a boundary  $\Gamma$  and in

**Fig. 1** Discretization of the original problem domain using finite elements and boundary elements

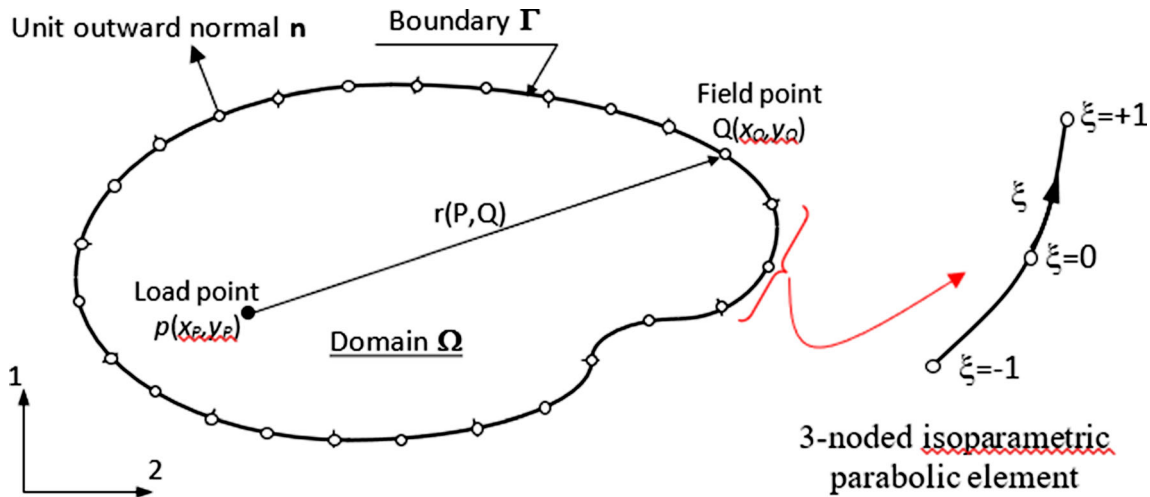
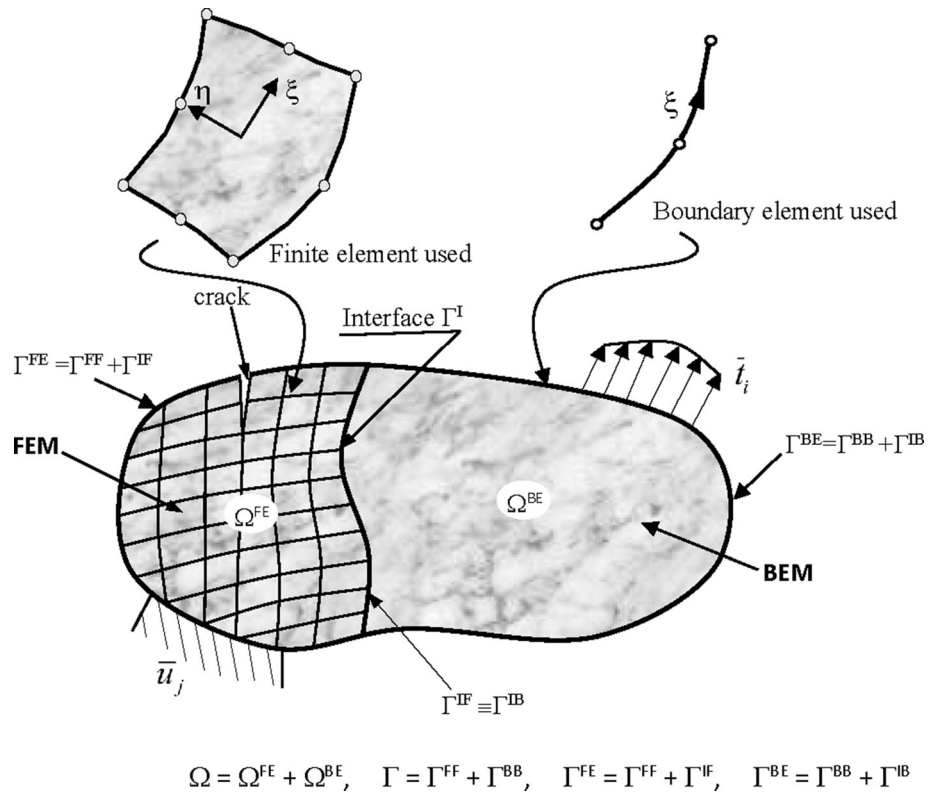


**Fig. 2** Discretization of two-dimensional domain boundary elements—load and field points relationship

the absence of the body forces, the displacement boundary integral equations for elasticity can be written as:

$$\mathbf{C}\mathbf{u}(p) + \int_{\Gamma} \mathbf{T}(p, Q)\mathbf{u}(Q)d\Gamma = \int_{\Gamma} \mathbf{U}(p, Q)\mathbf{t}(Q)d\Gamma \quad (\text{Eq 3})$$

In Eq (3), also known as Somigliana identity, the matrix  $\mathbf{C}$  is  $2 \times 2$  matrix of constant values depend on the type of point  $p$  under consideration. If  $p$  is an internal point

$$\mathbf{C} = \begin{bmatrix} 1 & 0 \\ 0 & 1 \end{bmatrix} \quad (\text{Eq 4})$$

If  $p$  is a boundary point on smooth surface then,

$$\mathbf{C} = \begin{bmatrix} \frac{1}{2} & 0 \\ 0 & \frac{1}{2} \end{bmatrix} \quad (\text{Eq 5})$$

If  $p$  is a corner with subtended angle  $\alpha$ , the matrix  $\mathbf{C}$  is given by [38],

$$\mathbf{C} = \begin{bmatrix} c_{11} & c_{12} \\ c_{21} & c_{22} \end{bmatrix} \tag{Eq 6}$$

with

$$c_{11} = -1 + \frac{1}{4\pi(1-\nu)} \left[ (2-2\nu)\alpha + \frac{\sin 2\alpha}{2} \right] \tag{Eq 7.a}$$

$$c_{22} = -1 + \frac{1}{4\pi(1-\nu)} \left[ (2-2\nu)\alpha - \frac{\sin 2\alpha}{2} \right] \tag{Eq 7.b}$$

$$c_{12} = c_{21} = -\sin^2 \alpha \tag{Eq 7.c}$$

The kernels  $\mathbf{T}(p, Q)$  and  $\mathbf{U}(p, Q)$  are matrices containing fundamental solutions for the tractions and displacements at point  $p$  on the boundary. Fundamental solutions are analytical solutions of the differential equations of elasticity for point forces at  $p$  in an infinite medium (Kelvin’s solutions). For two-dimensional plane strain problems, these kernels are given as [2]:

$$U_{ij}(p, Q) = \frac{1}{8\pi(1-\nu)G} \left[ (3-4\nu)\delta_{ij} \ln \frac{1}{r} + \frac{\partial r \partial r}{x_i x_j} \right] \tag{Eq 8}$$

$$T_{ij}(p, Q) = \frac{-1}{4\pi(1-\nu)r} \left\{ \frac{\partial r}{\partial n} \left[ (1-2\nu)\delta_{ij} + 2 \frac{\partial r \partial r}{\partial x_i \partial x_j} \right] - (1-2\nu) \left( \frac{\partial r}{\partial x_j} n_i - \frac{\partial r}{\partial x_i} n_j \right) \right\} \tag{Eq 9}$$

In which  $\delta_{ij}$  is the Kronecker delta,  $G$  is the shear modulus of the material, and  $r$  is the position vector, i.e., distance between point source and point field (see Fig. 1).

Substituting (1) into the matrix equation (3), we can write for each particular node, “ $i$ ”:

$$\mathbf{C}^i \mathbf{u}^i(p) + \sum_{j=1}^M \left[ \int_{\Gamma_j} \mathbf{T}(p, Q) \mathbf{N}(\xi) d\Gamma \right] \mathbf{u}^e = \sum_{j=1}^M \left[ \int_{\Gamma_j} \mathbf{U}(p, Q) \mathbf{N}(\xi) d\Gamma \right] \mathbf{t}^e \tag{Eq 10}$$

where  $M$  is the number of boundary elements, and  $\Gamma_e$  is the surface of the boundary element.

Now by means of nodal collocation and integration over the boundary elements, the boundary integral equations are transformed into the linear algebraic equations. As the collocation point passes through all the nodal points, the following system of linear algebraic equations is obtained:

$$[\mathbf{T}]\{\mathbf{u}_n\} = [\mathbf{U}]\{\mathbf{t}_n\} \tag{Eq 11}$$

where  $[\mathbf{T}]$  and  $[\mathbf{U}]$  denote the influence coefficients matrices which are obtained by integration over the boundary elements using the fundamental solutions, and  $\{\mathbf{u}_n\}$  and  $\{\mathbf{t}_n\}$  contain boundary displacements components and boundary tractions, respectively.

The final step is to specify the boundary conditions at each of the  $M$  nodes, and then, the system of Eq 11 can be reordered in such a way all the unknowns are written on the left-hand side in an  $\{\mathbf{Y}\}$  vector, and the knowns on the right-hand side in an  $\{\mathbf{z}\}$  vector to obtain the following final system.

$$[\mathbf{A}]\{\mathbf{Y}\} = \{\mathbf{z}\} \tag{Eq 12}$$

which may be solved for unknown nodal quantities,  $\{\mathbf{Y}\}$ . Once the values of displacements and tractions are known on the boundary, it is possible to calculate the displacements and stresses at any interior point using the expression [2]:

$$\mathbf{u}^i = \int_{\Gamma} \mathbf{U}(p, Q) \mathbf{t}(Q) d\Gamma - \int_{\Gamma} \mathbf{T}(p, Q) \mathbf{u}(Q) d\Gamma \tag{Eq 13}$$

$$\boldsymbol{\sigma}(p) = \int_{\Gamma} \mathbf{D}_{ij}(p, Q) \mathbf{t}(Q) d\Gamma - \int_{\Gamma} \mathbf{S}_{ij}(p, Q) \mathbf{u}(Q) d\Gamma \tag{Eq 14}$$

where

$$\mathbf{D}_{ij} = [\mathbf{D}_{1ij} \quad \mathbf{D}_{2ij}] \quad \text{and} \quad \mathbf{S}_{ij} = [\mathbf{S}_{1ij} \quad \mathbf{S}_{2ij}] \tag{Eq 15}$$

The values of the coefficients are:

$$D_{kij}(p, Q) = \frac{1}{4\pi(1-\nu)} \left( \frac{1}{r} \right) \left\{ (1-2\nu) \left[ \delta_{ki} \frac{\partial r}{\partial x_j} + \delta_{kj} \frac{\partial r}{\partial x_i} - \delta_{ij} \frac{\partial r}{\partial x_k} \right] + 2 \frac{\partial r}{\partial x_i} \cdot \frac{\partial r}{\partial x_j} \cdot \frac{\partial r}{\partial x_k} \right\} \tag{Eq 16}$$

$$S_{kij}(p, Q) = \frac{G}{2\pi(1-\nu)} \left( \frac{1}{r^2} \right) \left\{ 2 \frac{\partial r}{\partial n} \left[ (1-2\nu)\delta_{ij} \frac{\partial r}{\partial x_k} + \nu \left( \delta_{ik} \frac{\partial r}{\partial x_j} - \delta_{jk} \frac{\partial r}{\partial x_i} \right) \right] - 4 \frac{\partial r}{\partial x_i} \cdot \frac{\partial r}{\partial x_j} \cdot \frac{\partial r}{\partial x_k} \right. \\ \left. + 2\nu \left( n_i \frac{\partial r}{\partial x_j} \frac{\partial r}{\partial x_k} + n_j \frac{\partial r}{\partial x_i} \frac{\partial r}{\partial x_k} \right) + (1-2\nu) \left[ 2n_k \frac{\partial r}{\partial x_i} \cdot \frac{\partial r}{\partial x_j} + n_i \delta_{ik} + n_j \delta_{jk} \right] - (1-4\nu)n_k \delta_{ij} \right\} \tag{Eq 17}$$

### Finite Element Modeling of Elastoplastic Subdomain

The main goal of this paragraph is to give an overview of the application of FEM to the computation of the cracked region with material nonlinearity. A comprehensive bibliography on the finite element method and nonlinearity will be found in Zienkiewicz and Taylor [1]. Indeed, the basic formulation applied to linear elastic theory can be used for nonlinear elastoplastic deformation of solids induced by small load increments. All physical quantities, including the displacements, strains, stresses, and strain energy, will



be dealt with in the incremental sense. As a result, following the usual discretization prescribed in finite element analysis, we obtain the expressions of the incremental displacements within any element,  $\{\Delta \mathbf{u}\}^e$ , which are given by

$$\{\Delta \mathbf{u}\}^e = [\mathbf{N}]\{\Delta \mathbf{u}_n\} \quad (\text{Eq 18})$$

where  $[\mathbf{N}]$  is the usual matrix of the shape functions, and  $\{\Delta \mathbf{u}_n\}$  is the incremental displacement vector at the nodes.

The incremental strains in an element can be related to the incremental displacement vector  $\{\Delta \mathbf{u}_n\}$  at the nodes by the deformation matrix  $[\mathbf{B}]$ :

$$\{\Delta \boldsymbol{\varepsilon}\}^e = [\mathbf{B}]\{\Delta \mathbf{u}_n\} \quad (\text{Eq 19})$$

The incremental stress–strain relationship can be also expressed in an incremental way as:

$$\{\Delta \boldsymbol{\sigma}\}^e = [\mathbf{D}_{ep}]\{\Delta \boldsymbol{\varepsilon}\}^e \quad (\text{Eq 20})$$

where  $[\mathbf{D}_{ep}]$  is the elastoplastic stress–strain matrix which defines the incremental relationship between stress and total strain and depends on the level of stress. A detailed description on the determination of the matrix  $[\mathbf{D}_{ep}]$  can be found in Owen and Fawkes [39].

The incremental strain energy in the element can be formulated as:

$$\{\Delta U\}^e = \frac{1}{2} \int_{\Omega_e} \{\Delta \boldsymbol{\varepsilon}\}^T \{\Delta \boldsymbol{\sigma}\} d\Omega_e \quad (\text{Eq 21})$$

Replacing  $\{\Delta \boldsymbol{\varepsilon}\}^e$  and  $\{\Delta \boldsymbol{\sigma}\}^e$ , respectively, by Eqs 19 and 20, the above expression for  $\{\Delta U\}^e$  can be expressed in terms of  $\{\Delta \mathbf{u}_n\}$  as

$$\{\Delta U\}^e = \frac{1}{2} \{\Delta \mathbf{u}_n\}^T \left( \int_{\Omega_e} [\mathbf{B}]^T [\mathbf{D}_{ep}] [\mathbf{B}] \right) \{\Delta \mathbf{u}_n\} d\Omega_e \quad (\text{Eq 22})$$

The incremental potential energy stored can be expressed as:

$$\{\Delta \Pi\} = \{\Delta U\} - \{\Delta W\} \quad (\text{Eq 23})$$

In which  $\{\Delta W\}$  is the work done on the element by external forces

$$\{\Delta W\} = \int_{\Omega_e} \{\Delta \mathbf{u}_n\}^T \{\Delta \mathbf{b}\} d\Omega_e + \int_{\Gamma_e} \{\Delta \mathbf{u}_n\}^T \{\Delta \mathbf{f}\} d\Gamma_e \quad (\text{Eq 24})$$

where  $\{\Delta \mathbf{b}\}$  is the increment body force, and  $\{\Delta \mathbf{f}\}$  is the increment external applied forces.

Upon substituting  $\{\Delta U\}$  in Eq 13 and  $\{\Delta W\}$  in Eq 24 into the expression for  $\{\Delta \Pi\}$  and applying the variational process to this quantity, with respect to  $\{\Delta \mathbf{u}_n\}$ , leads to the following set of equations

$$\frac{\partial(\Delta \Pi)}{\partial\{\Delta \mathbf{u}_n\}} = \left( \int_{\Omega_e} [\mathbf{B}]^T [\mathbf{D}_{ep}] [\mathbf{B}] d\Omega_e \right) \{\Delta \mathbf{u}_n\} - \int_{\Omega_e} \{\Delta \mathbf{b}\} d\Omega_e - \int_{\Gamma_e} \{\Delta \mathbf{f}\} d\Gamma_e = 0 \quad (\text{Eq 25})$$

The second portion of the above equality can be rearranged to give the following element equations:

$$[\mathbf{K}]^e \{\Delta \mathbf{u}_n\} = \{\Delta \mathbf{p}\} \quad (\text{Eq 26})$$

where

$$[\mathbf{K}]^e = \int_{\Omega_e} [\mathbf{B}] [\mathbf{D}_{ep}] [\mathbf{B}]^T d\Omega_e \quad (\text{Eq 27})$$

and

$$\{\Delta \mathbf{p}\} = \int_{\Omega_e} \{\Delta \mathbf{b}\} d\Omega_e + \int_{\Gamma_e} \{\Delta \mathbf{f}\} d\Gamma_e \quad (\text{Eq 28})$$

Are, respectively, the tangent stiffness matrix and the incremental elementary force vector.

The overall structure equation can be readily assembled from the element equation (26) as follows:

$$[\mathbf{K}]\{\Delta \mathbf{u}\} = \{\Delta \mathbf{R}\} \quad (\text{Eq 29})$$

where

$$[\mathbf{K}] = \sum_{e=1}^M [\mathbf{K}]^e \quad (\text{Eq 30})$$

$$\{\Delta \mathbf{R}\} = \sum_{e=1}^M \{\Delta \mathbf{p}\}^e \quad (\text{Eq 31})$$

In which  $M$  is equal to the total number of elements in the structure.

Equation 29 will not generally be satisfied at any stage of the computation because of the nonlinearity of the stiffness matrix, and the residual forces is given by:

$$\{\Delta \boldsymbol{\psi}\} = [\mathbf{K}]\{\Delta \mathbf{u}\} - \{\Delta \mathbf{R}\} \neq \mathbf{0} \quad (\text{Eq 32})$$

Standard solution procedure, at each load increment, contains iterations over computations of tangent stiffness (based on current temperature, stress, and plastic strain, if required), applied loads based on current configuration, internal force, and residual force. Then, displacement increment is calculated. With updated displacements, the plastic strain increments at element integration points are obtained. Finally, check on convergence is carried out. If the procedure converged, plastic strains are updated and next increment proceeds.

### Use of J-Integral in Elastoplastic Fracture

Applications of the finite element method to nonlinear fracture mechanics are well documented. In fact, several approaches have been proposed in the literature for fracture prediction in ductile materials [40, 41], but the J-integral technique proposed by Rice [42] is currently the most popular and widely accepted [39]. The aim of this section is to describe how the J-contour integral can be employed in elastoplastic fracture problems. Indeed, the J-integral is also an effective method for the determination of stress intensity factors. From Fig. 3, it can be shown that the J-integral, is independent of the actual path chosen, provided that the initial and end points of the contour  $\Gamma$  are on opposite faces of the crack and that the contour contains the crack tip.

$$J = \int_{\Gamma_J} \left( U dy - t_i \frac{\partial u_i}{\partial x_i} ds \right) \tag{Eq 33}$$

where  $U$  denotes the strain energy density,  $u_i$  is the displacements vector, and  $t_i$  represents the tractions vector along the elementary arc  $ds$  of the integration contour  $\Gamma_J$ . The relationship between the J-integral and the stress intensity factors is given by:

$$J^I = \frac{K_I^2}{E'}, \quad J^{II} = \frac{K_{II}^2}{E'}, \tag{Eq 34}$$

where the constant  $E'$  is the elasticity modulus  $E$  for plane stress conditions and  $E' = E/(1 - \nu^2)$  for plane strain conditions.

Application of the J-integral to elastoplastic fracture stems from the solutions derived by Rice and Rosengren [43] and Hutchinson [44]. These solutions give the stress and plastic strain fields ahead of a crack in a power-hardening material obeying the laws of total deformation plasticity to be [39]:

$$\sigma_{ij} \propto \left( \frac{J}{\sigma_Y r} \right)^{h/h+1} f_{ij}(\theta), \quad \varepsilon_{ij} \propto \left( \frac{J}{\sigma_Y r} \right)^{1/h+1} f_{ij}(\theta) \tag{Eq 35}$$

Where  $\sigma_Y$  the material yield stress, and  $h$  is the hardening exponent.

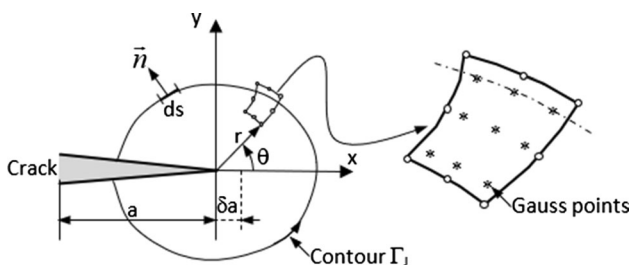


Fig. 3 Contour path for J-integral evaluation

For elastoplastic problems, the J-integral has been numerically evaluated by employing the appropriate definition of the strain energy density,  $U$ . Separating  $U$  into its elastic and plastic components

$$U = U_e + U_p \tag{Eq 36}$$

then  $U_e$  is given by

$$U_e = \frac{1}{2} \sigma_{ij} (\varepsilon_{ij})_e \tag{Eq 37}$$

where  $(\varepsilon_{ij})_e$  denotes the elastic components of strain. The plastic work contribution is given by

$$U_p = \int_0^{\bar{\varepsilon}_p} \bar{\sigma} d\bar{\varepsilon}_p \tag{Eq 38}$$

in which  $\bar{\sigma}$  and  $\bar{\varepsilon}_p$  are the effective stress and effective plastic strain, respectively.

### FEM–BEM Coupling Procedure

In this section, the interface relaxation procedure for FEM–BEM coupling presented by Lin et al. [45] and Parera and Alarcon [35] will be extended to resolve the two-dimensional elastoplastic fracture mechanics. Indeed, this method

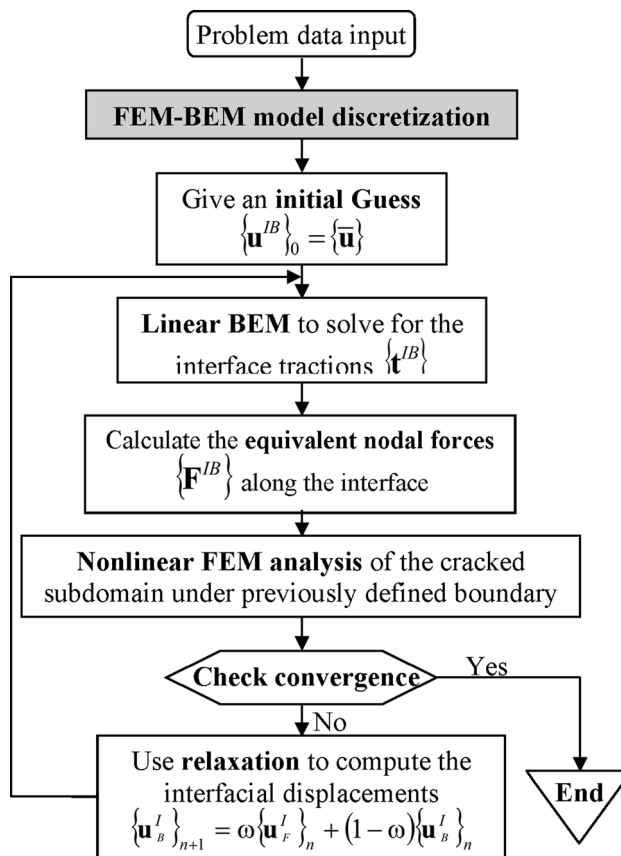
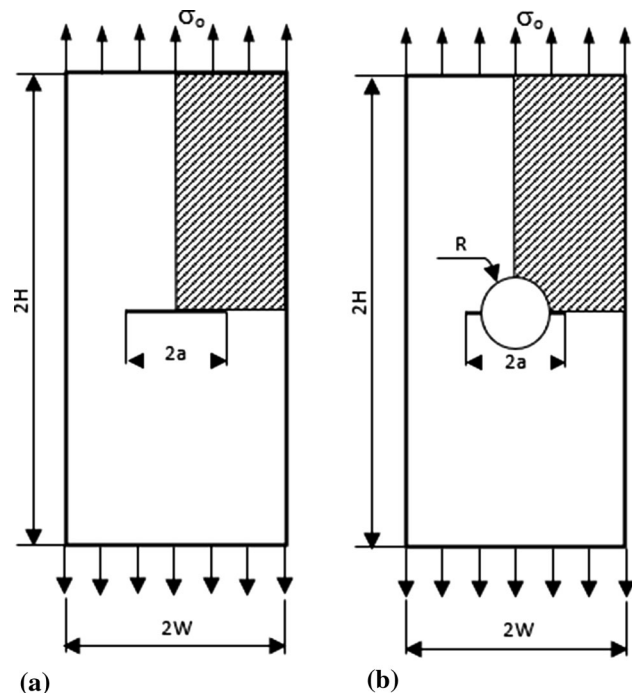


Fig. 4 Algorithm of FEM–BEM coupling for elasto-plastic fracture

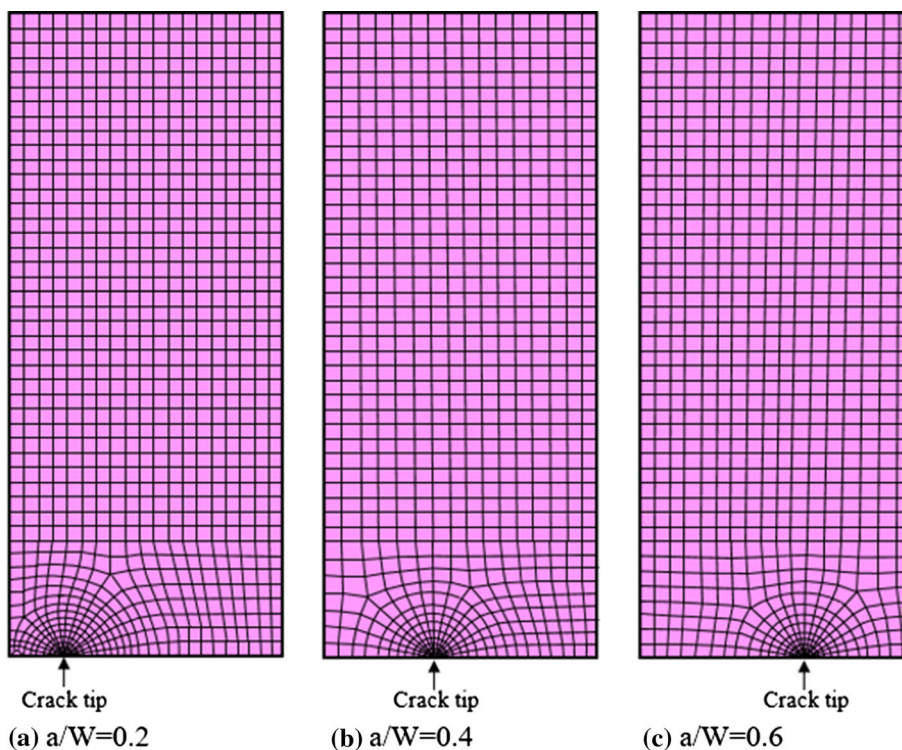
was investigated recently by several authors in different applications [35, 46, 47].

The principle of this procedure is based on the subdivision of the original problem into two subregions. By this approach, we resolve the differential equations in separate



**Fig. 5** Cracked plate with: (a) central crack, (b) cracks emanating from a circular hole

**Fig. 6** FEM meshes of the plate with central crack for different crack lengths



meshes and we calculate the equivalent nodal forces to tractions obtained by BEM at the interface. These latter will be used as boundary conditions to FEM subdomain to solve for the interfacial displacements. The procedure is then iterated until convergence is achieved. Noting that to accelerate convergence, at each iteration, a relaxation is accomplished at the interface using the following relationship:

$$\{u_B^I\}_{n+1} = \omega \{u_F^I\}_n + (1 - \omega) \{u_B^I\}_n \tag{Eq 39}$$

where  $\{u_F^I\}_n$  and  $\{u_B^I\}_n$  being, respectively, the available FEM and BEM displacements at the interface in the  $n^{th}$  iteration, and  $\omega$  is a relaxation parameter, which can be constant or selected dynamically by means of a simple formula to maximize the rate of convergence of the above iteration [45]. In all the calculations carried out in this work, we have adopted a dynamic relaxation parameter.

Equations systems (11) and (32) obtained from both methods can be rewritten by their partitions into those associated with the interface, and disassociated from the interface as follows

$$\begin{bmatrix} H_{11} & H_{12} \\ H_{21} & H_{22} \end{bmatrix} \begin{Bmatrix} u_B^B \\ u_B^I \end{Bmatrix} = \begin{bmatrix} G_{11} & G_{12} \\ G_{21} & G_{22} \end{bmatrix} \begin{Bmatrix} t_B^B \\ t_B^I \end{Bmatrix} \tag{Eq 40}$$

for BEM subdomain

$$\begin{Bmatrix} \Delta \Psi_F^F \\ \Delta \Psi_F^I \end{Bmatrix} = \begin{bmatrix} K_{T11} & K_{T12} \\ K_{T21} & K_{T22} \end{bmatrix} \begin{Bmatrix} \Delta u_F^F \\ \Delta u_F^I \end{Bmatrix} - \begin{Bmatrix} \Delta F_F^F \\ \Delta F_F^I \end{Bmatrix} \tag{Eq 41}$$

For the FEM subdomain



**Fig. 7** FEM–BEM meshes of the plate with central crack for different crack lengths

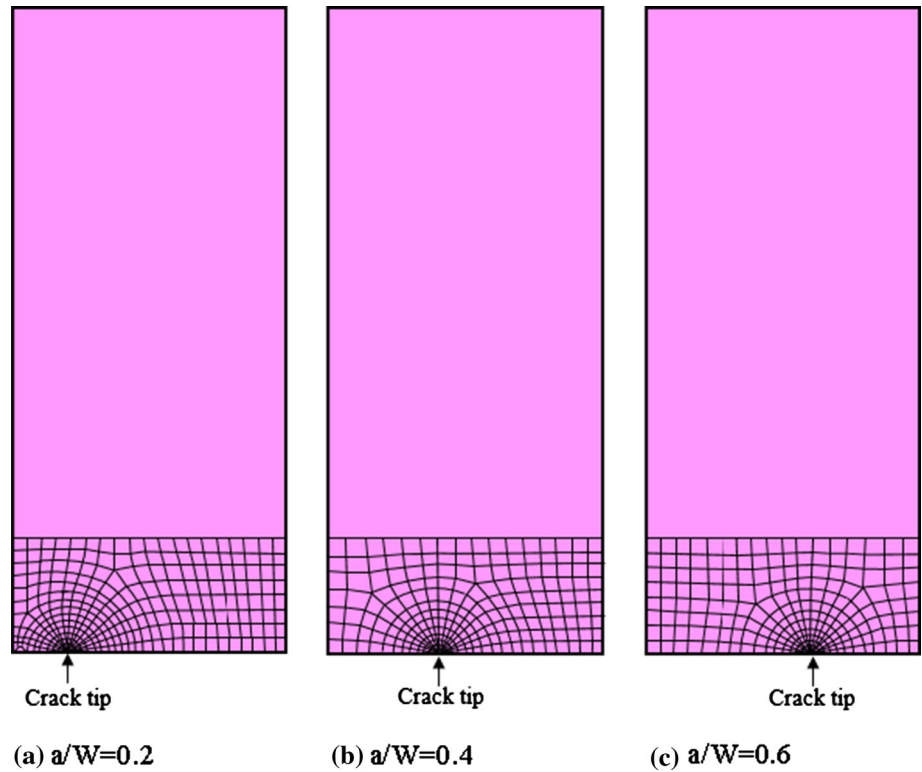


**Fig. 8** Evolution of J-integral as a function of normalized stress for different values of  $a/W$  in the case of a plate with central crack under plane stress conditions

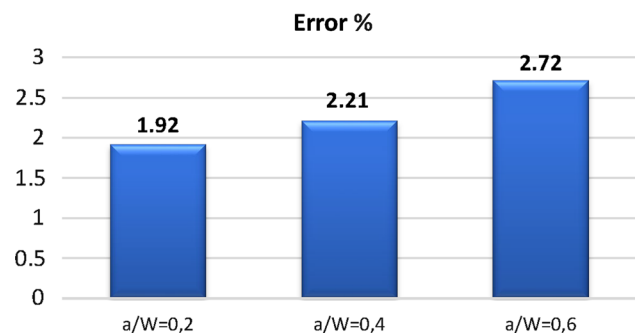
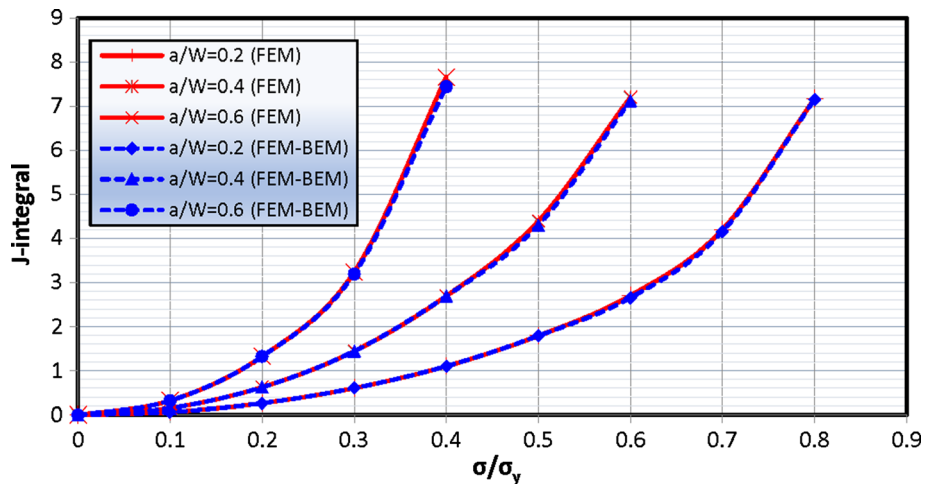


**Fig. 9** The maximum relative error between the normalized stresses obtained by FEM and FEM–BEM

where subscripts F, B and I represent finite element, boundary element and interface, respectively.

The original problem is restored by coupling the subdomain which is discretized by finite elements and the other subdomain modeled by boundary elements, by satisfying the equilibrium and the compatibility conditions along the interface between both subdomains, i.e.,

$$u_B^I = u_F^I \quad \text{on } \Gamma^I \tag{Eq 42}$$

$$F_B^I + F_F^I = \mathbf{0} \quad \text{on } \Gamma^I \tag{Eq 43}$$

**Fig. 10** CPU time for the elastoplastic analysis of the central crack plate

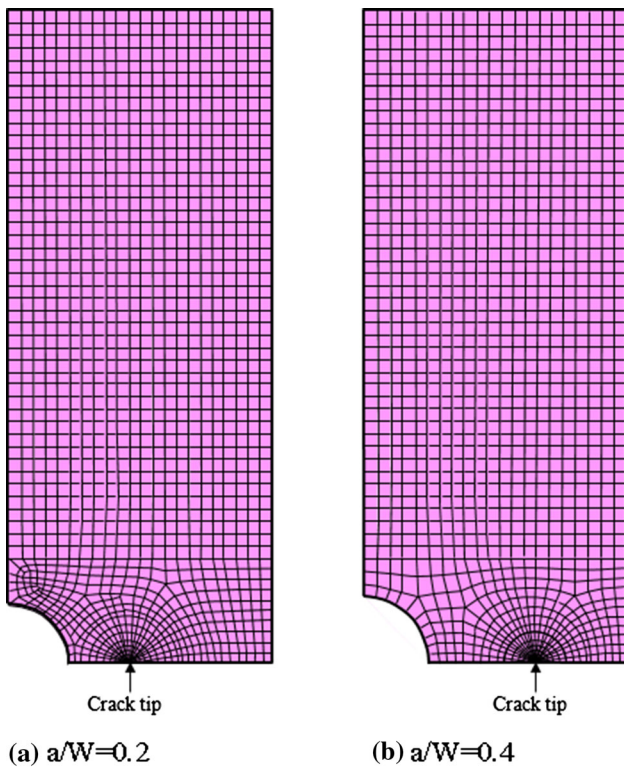
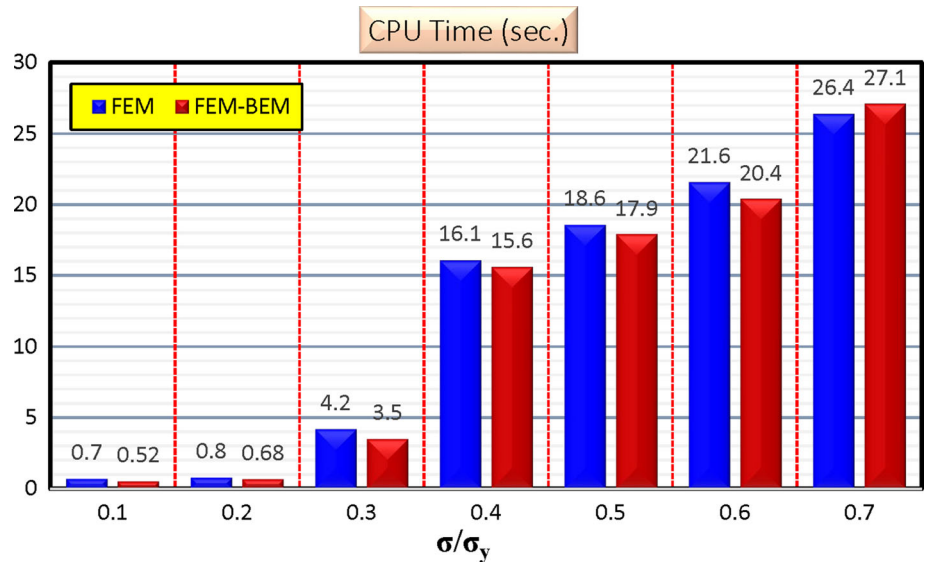


**Fig. 11** FEM meshes of the perforated plate in uniaxial tension with a crack emanating from a hole for two different crack lengths: (a)  $a/W = 0.2$  and (b)  $a/W = 0.4$

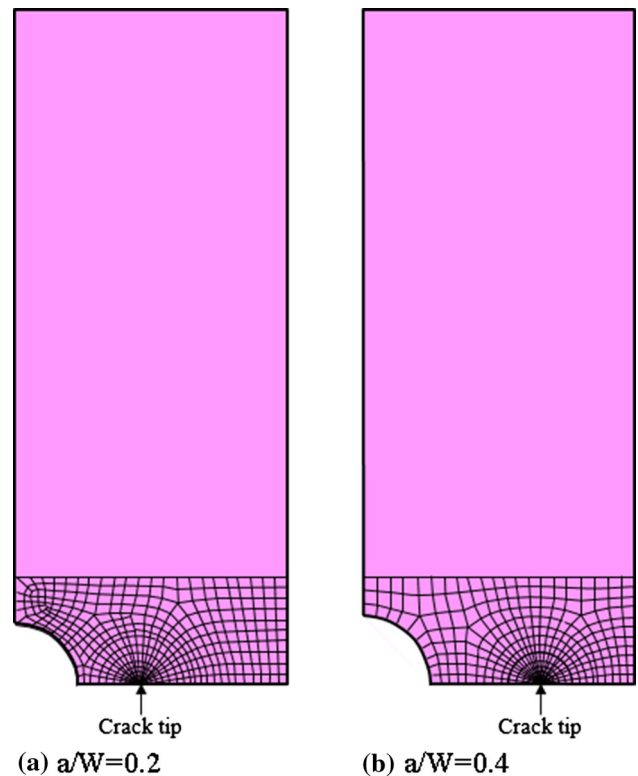


**Fig. 12** FEM–BEM meshes of the perforated plate in uniaxial tension with a crack emanating from a hole for two different crack lengths: (a)  $a/W = 0.2$  and (b)  $a/W = 0.4$

where  $\{\mathbf{F}_B^I\} = [\mathbf{M}]\{\mathbf{t}_B^I\}$  is the nodal forces vector obtained in terms of surface tractions by using the principle of virtual work along the interface.  $[\mathbf{M}]$  is the converting matrix due to the weighing of the boundary tractions by the

interpolation functions on the interface (see Aour et al. [17]).

The order by which the functional blocks characterizing the proposed coupling method are called, may be summarized as indicated in Fig. 4.

**Fig. 13** Evolution of the J-integral as a function of normalized stress for  $a/W = 0.2$  and  $0.4$  in the case of a perforated plate in uniaxial tension with a crack emanating from a hole under plane stress conditions

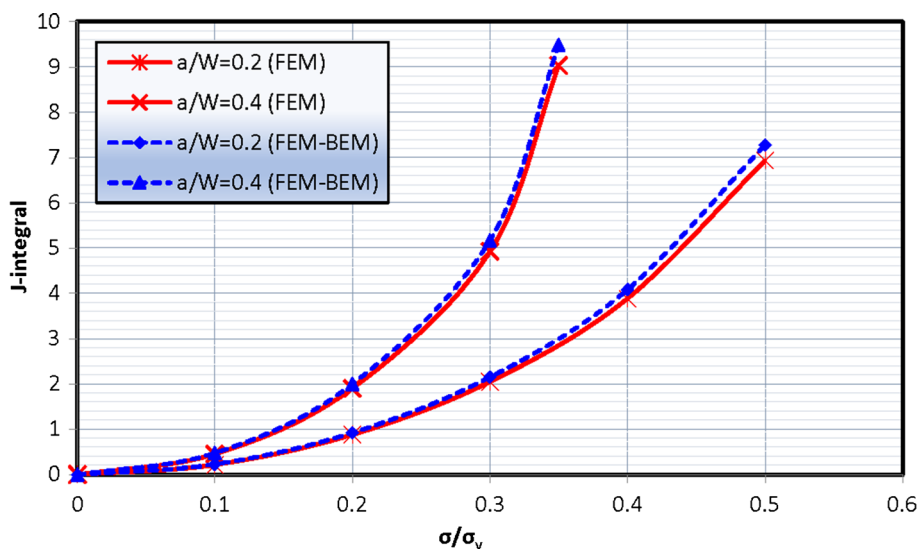
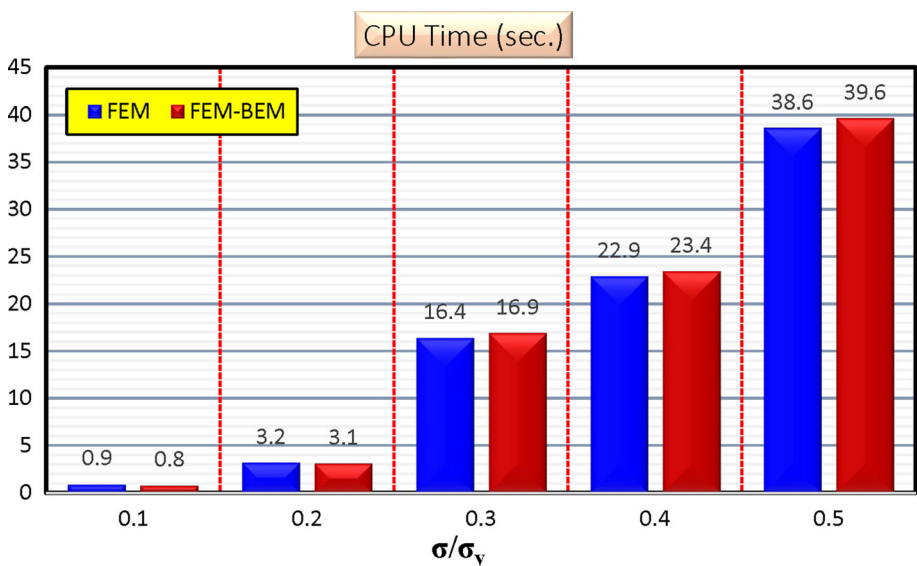


**Fig. 14** CPU time for the elastoplastic analysis of the perforated plate with a crack emanating from a hole



It should be noted that the coupling method presented here seems to be easier and more efficient than other methods (FE hosted and BE hosted), since the user need not have any access to the computer codes, and it allows to maintain all the advantageous numerical features of the FEM matrix. Indeed, only interface information, such as interface forces and displacements, needs to be communicated between both programs.

**Results and Discussion**

To highlight the reliability and efficiency of the developed FEM–BEM coupling method, we will present, in what follows, the analysis of three problems of nonlinear fracture mechanics. The first one concerns a plate with a

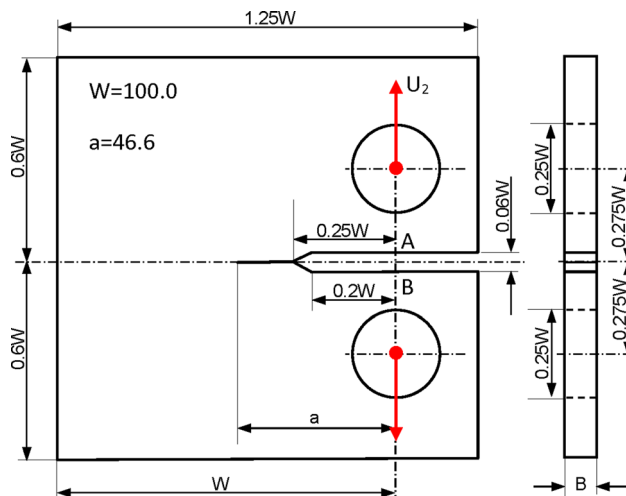


**Fig. 15** Geometry of compact tension specimen

central crack, the second one concerns a plate composed of two symmetrical cracks emanating from a circular hole in the center, and the third is reserved for the problem of a compact specimen. Since the material is plastic in the vicinity of the crack, FEM is used in this region since it is more suitable for modeling nonlinear regions, whereas the remaining part of the structure which is linear elastic is easily modeled by BEM. The developed FEM–BEM software was designed to be general enough to solve plane strain/stress problems with elastoplastic failure behavior. For all numerical simulations performed, the obtained results have been compared with those provided by FEM.

#### Center Cracked Plate

The example of center cracked plate under uniaxial tensile is presented as a first numerical test. This problem has been used by several authors [17, 48] as a benchmark because an analytical solution is available [49]. The geometry and loading assumed in this example are shown in Fig. 5a. The criterion of Von Mises with a state of plane stress was assumed. This problem was analyzed considering a perfectly plastic elastic behavior. The material properties employed are as follows: Young's modulus  $E = 10000\text{MPa}$ , Poisson's ratio  $\nu = 0.3$ , tensile yield stress  $\sigma_Y = 100\text{MPa}$ .

Due to the symmetry of the problem, only one quarter of the plate needs to be modeled. The meshes used for FEM and the coupled FEM–BEM analysis for crack lengths  $a/W = 0.2, 0.4$  and  $0.6$  are indicated in Figs. 6 and 7, respectively. Note that the mesh size was chosen after a mesh sensitivity study. Furthermore, the same element size has been chosen for both FEM and FEM–BEM meshes so that a fair comparison can be made.

Figure 8 shows the evolution of J-integral versus normalized stress  $\sigma/\sigma_y$  under a plane stress condition for different values of  $a/W = \{0.2, 0.4, 0.6\}$  obtained by FEM and FEM–BEM. The results of FEM–BEM coupling method are in good agreement with those of FEM for different loading and different crack lengths.

To compare the FEM and the FEM–BEM, the relative error was defined as follows:

$$\text{Error}\% = \frac{\text{Sol}_{\text{FEM}} - \text{Sol}_{\text{FEM-BEM}}}{\text{Sol}_{\text{FEM}}} \times 100 \quad (\text{Eq 44})$$

As you can see from Fig. 9, the maximum relative errors obtained for crack lengths  $a/W = 0.2, 0.4$  and  $0.6$  are, respectively, equal to 1.92, 2.21 and 2.72%.

Figure 10 illustrates the time required to complete the FEM and FEM–BEM calculations for different stress ratios. It can be noted that the CPU time for FEM–BEM is relatively small compared to that of FEM for most of the stress values, except for the last case ( $a/w = 0.7$ ), where it

becomes slightly higher. Note that the CPU time of the FEM–BEM coupling can be further reduced by using two processors treating both subdomains in parallel and a work on this subject is under investigation.

#### Perforated Plate with a Crack Emanating from the Hole

This problem represents the analysis of a perforated plate with the existence of a crack emanating from a hole, in a plane stress state. The plate has been analyzed considering a perfectly plastic elastic behavior with the following material properties: Young's modulus  $E = 10000\text{MPa}$ , Poisson's ratio = 0.3 and yield stress  $\sigma_Y = 100\text{MPa}$ . The Von Mises criterion was adopted. The J-integral was evaluated for two different crack lengths  $a=2\text{mm}$  and  $4\text{mm}$  as a function of the evolution of the applied load. The FEM and FEM–BEM analyses were performed with the mesh models shown in Figs. 11 and 12, respectively.

The evolution of J-integral as a function of the normalized stress  $\sigma/\sigma_y$  in the mentioned state of plane stress, for  $a/W = 0.2$  and  $0.4$  using the finite element method and the iterative FEM–BEM coupling method is shown in Fig. 13. The coupled FEM–BEM method matches very well with the FEM solutions for both values of  $a/W$  under the load intensities and material constants considered. Indeed, the relative error for both types of crack length does not exceed 5%.

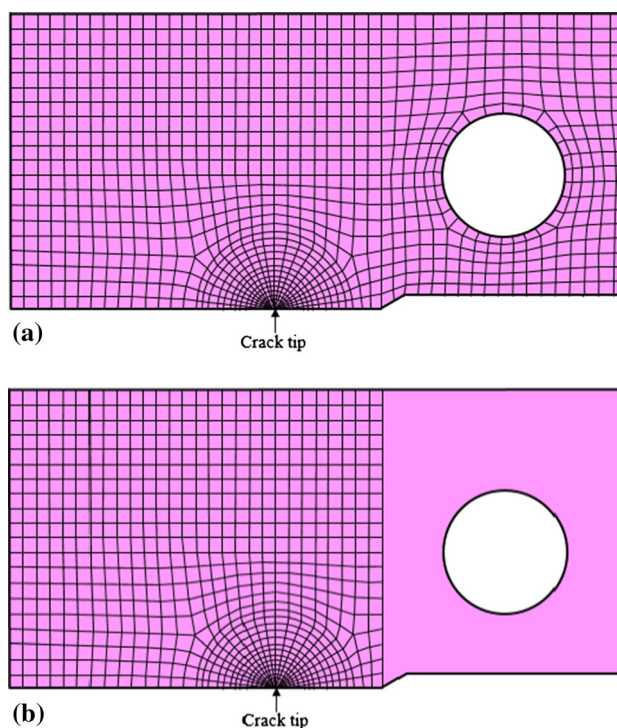


**Fig. 16** Discretization used in (a) FEM and (b) coupled FEM–BEM analysis (mesh A)

**Fig. 17** Evolution of the normal stress along the x-axis from the crack tip

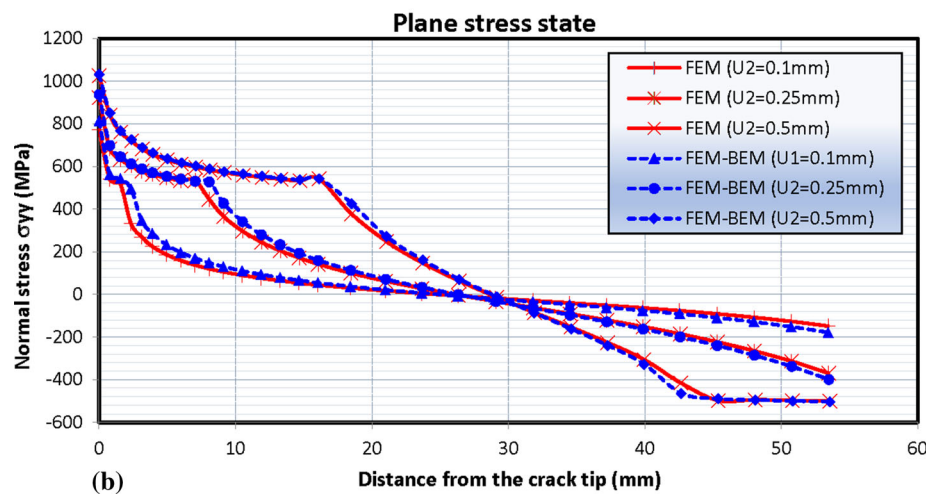
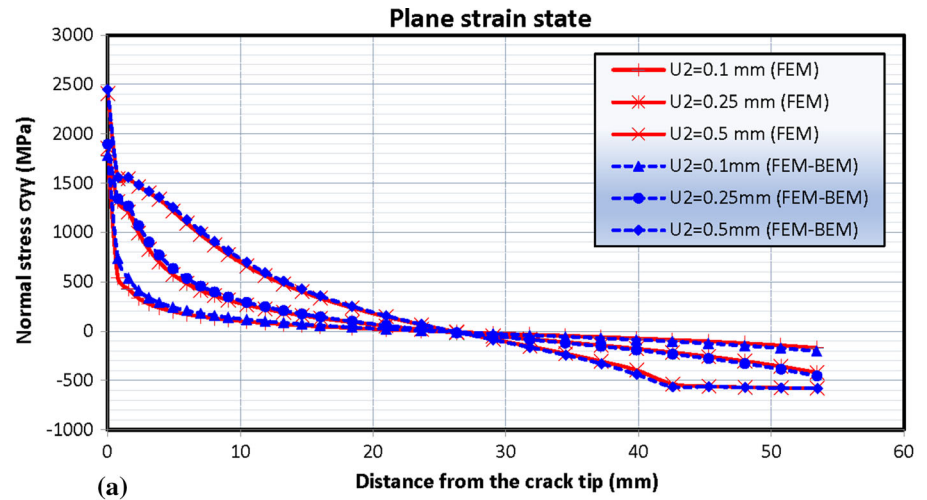
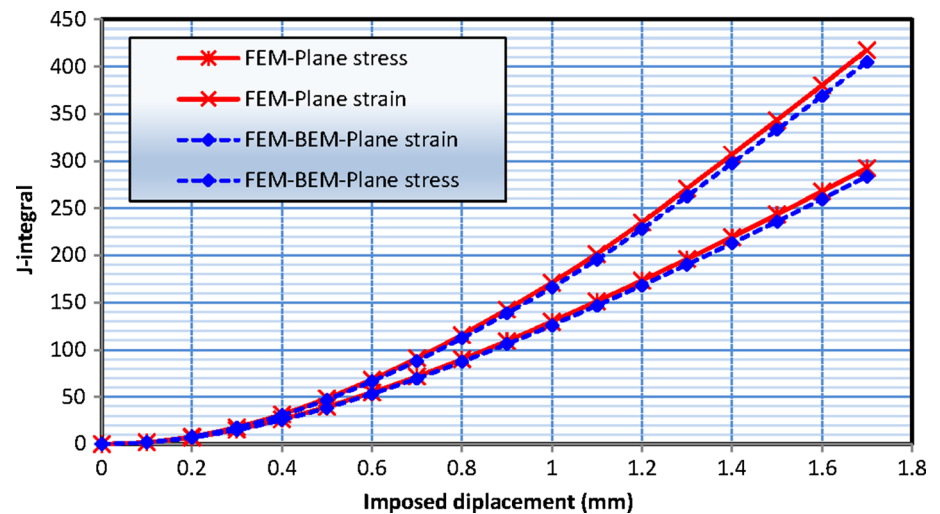


**Fig. 18** Evolution of J-integral as a function of the imposed displacement in the case of a compact specimen in uniaxial tension in plane strain and plane stress states



The time required for the analysis with FEM and FEM-BEM methods, for various values of  $\sigma_y/\sigma$ , is presented in Fig. 14. From this histogram, the difference in CPU time

recorded for both methods is not significant since the analyzed problem is elastic perfectly plastic and without using parallel processors.



### Compact Tensile Specimen

This example describes the application of the coupled FEM–BEM analysis to the problem of a compact tension specimen whose geometry is shown in Fig. 15. This specimen had previously been the subject of an experimental investigation [50] and extensive plasticization occurred prior to unstable fracture. The relationship between applied load and the clip gauge measuring the displacements at the load line between the points AB on the machined notch had been experimentally recorded. This problem has also been numerically analyzed by several other investigators in a comparative study [39]. Material parameters used are as follows: Young’s modulus  $E = 210.915 \text{ KN/mm}^2$ , Poisson’s ratio  $\nu = 0.33$ , tensile yield stress  $\sigma_Y = 0.48843 \text{ KN/mm}^2$ .

The finite element mesh of one half of the specimen employed in analysis is shown in Fig. 16a and contains 1140 8-node quadratic elements. A relatively refined mesh was used in the vicinity of the crack tip. Zero displacements

in the y-direction are imposed on the nodes located in the uncracked lower part. A displacement  $U_2$  was also imposed, along the direction of loading (see Fig. 15). Plane stress and strain states were considered. The values of the effective stress–effective strain curve have been introduced into the simulation. Figure 16b shows the mesh used for the FEM–BEM simulation. The first subregion containing the crack, where are awaited elastoplastic deformations, has been discretized by FEM using 844 FE. The second subregion has been modeled by BEM using 100 BE.

Figure 17 shows the variation of the normal stresses  $\sigma_{yy}$  at the crack plane, along the x-axis from the crack tip, in plane strain and plane stress states, respectively. A good agreement between the FEM and FEM–BEM results was found for the three selected values of imposed displacements ( $U_2 = 0.1, 0.25$  and  $0.5 \text{ mm}$ ).

Figure 18 shows the evolution of the J-integral as a function of the imposed displacement in the case of plane stress and plane strain. A comparison between the results obtained by FEM and those of FEM–BEM coupling has also been presented. There is a good agreement between the curves of both methods, proving again the validity and reliability of the proposed coupling method.

To highlight the effect of the mesh on the FEM–BEM computation time, a second mesh consisting of 536 finite elements coupled with 156 boundary elements was examined (see Fig. 19). The comparison between the computation times in the plane stress state, for both FEM and FEM–BEM methods using both meshes presented in Figs. 16 and 19, is presented in Fig. 20. There is a slight reduction in computation time by shrinking the FEM subdomain.

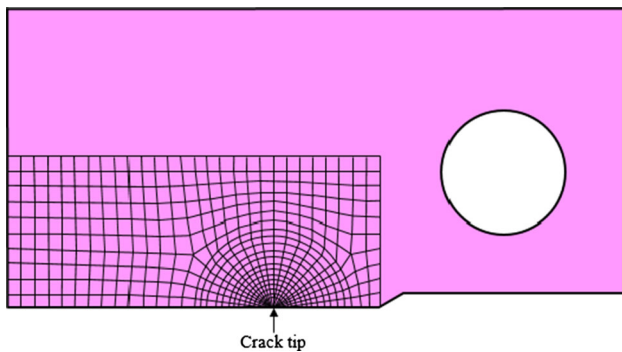
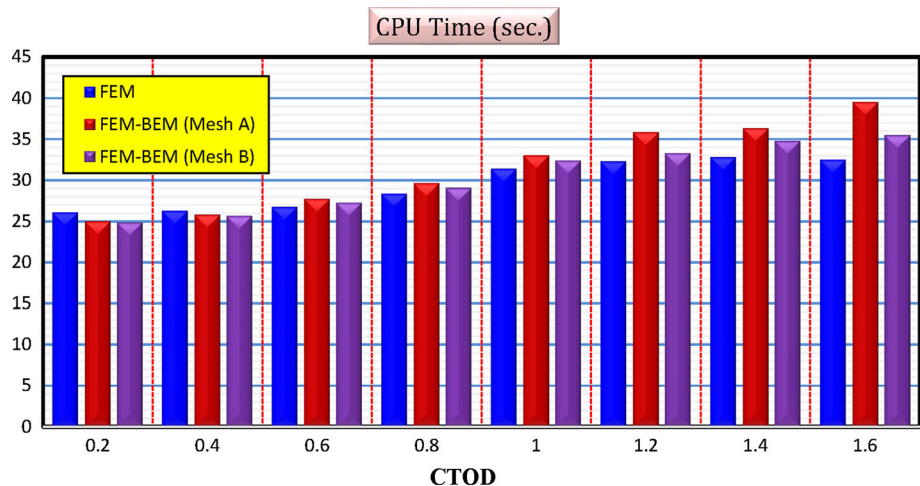


**Fig. 19** Second FEM–BEM mesh (Mesh B) of the compact tensile specimen used for the calculation of the CPU time

**Fig. 20** CPU time for the elastoplastic analysis of the compact specimen in the plane stress state



## Conclusion

In the framework of the development of a code for solving fracture mechanics problems, an extension of the iterative FEM–BEM coupling approach has been proposed in this paper. The finite element method was used for the calculation of the subdomain containing the crack, due to its ability to handle plastic zones and strong stress gradients, while the remaining subdomain, often linearly elastic, is analyzed by the boundary element method, which is well suited for this type of behavior and gives the advantage of reducing the part of the domain to be meshed.

To highlight the efficiency and the versatility of the proposed method and its accuracy compared to FEM, examples of problems with cracks, in elastoplastic behavior, have been solved. The comparison of the results obtained by FEM and FEM–BEM methods shows that the coupling method, in addition to its ability to deal with a wider range of problems, is much better in terms of accuracy and CPU time than the FEM since the number of arithmetic operations is greatly reduced.

It should be noted that the iterative FEM–BEM method has the advantage of conserving the characteristics of the FEM and BEM, and consequently, a different formulation can be implemented for each method without alteration of the global structure of computer codes. Therefore, one can say that the present coupling is a useful tool for realistic nonlinear applications, due to the preservation of merits and accuracy of each method and simplicity to directly use the different software packages.

In this paper, only two-dimensional solutions have been presented. The extension of the current coupled approach for three-dimensional is likely to be worthwhile because the benefits of reducing the size of the final system of equations are greater in three dimensions. Therefore, the coupled approach is more interesting in three-dimensional elastoplastic fracture mechanics, and research is continuing in this direction.

## References

- O.C. Zienkiewicz, R.L. Taylor, *The Finite Element Method*. (McGraw-Hill, London, 1991)
- C.A. Brebbia, J. Dominguez, *Boundary Elements: An Introductory Course*, 2nd edn. (Computational Mechanics Publications, 1992)
- O.C. Zienkiewicz, D.W. Kelly, P. Bettles, The coupling of the finite element method and boundary solution procedures. *Int. J. Numer. Methods Eng.* **11**, 355–375 (1977)
- G. Beer, Finite element, boundary element and coupled analysis of unbounded problems in elastostatics. *Int. J. Numer. Methods Eng.* **19**, 567–580 (1983)
- G.C. Hsiao, The coupling of BEM and FEM—a brief review, in *Boundary Element X, Computational Mechanics* (Southampton, 1988), pp. 431–445
- D. Boumaiza, B. Aour, On the efficiency of the Iterative coupling FEM–BEM for solving the elasto-plastic problems. *Eng. Struct.* **72**(2014), 12–25 (2014)
- C. Oysu, R.T. Fenner, Coupled FEM–BEM for elastoplastic contact problems using Lagrange multipliers. *Appl. Math. Model.* **30**, 231–247 (2005)
- D. Ji, W. Lei, Z. Liu, Finite element method and boundary element method iterative coupling algorithm for 2-D elastodynamic analysis. *Comput. Appl. Math.* (2020). <https://doi.org/10.1007/s40314-020-01233-4>
- S. Ganguly, J.B. Layton, C. Balakrishna, A coupling of multi-zone curved Galerkin BEM with finite elements for independently modelled sub-domains with non-matching nodes in elasticity. *Int. J. Numer. Methods Eng.* **59**, 1021–1038 (2004)
- C.A. Brebbia, P. Georgiou, Combination of boundary and finite elements in elastostatics. *Appl. Math. Model.* **3**, 212–220 (1979)
- B. Aour, *Couplage FEM-DBEM singulières pour l'analyse des problèmes d'élastostatique bidimensionnels*, Thèse de Magister, USTO, Oran, 1997
- C.Y. Dong, An iterative FE–BE coupling method for elastostatics. *Comput. Struct.* **79**, 293–299 (2001)
- W. Elleithy, R. Grzhibovskis, An adaptive domain decomposition coupled finite element-boundary element method for solving problems in elasto-plasticity. *Int. J. Numer. Methods Eng.* **2009**(79), 1019–1040 (2009)
- A.D. Mesquita, H.B. Coda, A two-dimensional BEM/FEM coupling applied to viscoelastic analysis of composite domains. *Int. J. Numer. Methods Eng.* **2003**(57), 251–270 (2003). <https://doi.org/10.1002/nme.676>
- N. Troyani, A. Pérez, A comparison of a finite element only scheme and a BEM/FEM method to compute the elastic–viscoelastic response in composite media. *Finite Elem. Anal. Des.* **88**(2014), 42–54 (2014)
- D. Soares Jr., J.C.F. Telles, W.J. Mansur, Boundary elements with equilibrium satisfaction—a consistent formulation for dynamic problems considering non-linear effects. *Int. J. Numer. Methods Eng.* **2006**(65), 701–713 (2006)
- B. Aour, O. Rahmani, M. Nait-Abdelaziz, A coupled FEM/BEM approach and its accuracy for solving crack problems in fracture mechanics. *Int. J. Solids Struct.* **44**, 2523–2539 (2007)
- G.E. Bird, J. Trevelyan, C.E. Augarde, A coupled BEM/scaled boundary FEM formulation for accurate computations in linear elastic fracture mechanics. *Eng. Anal. Bound. Elem.* **34**(6), 599–610 (2010)
- R. Citarella, V. Giannella, E. Vivo, M. Mazzeo, FEM–DBEM approach for crack propagation in a low pressure aeroengine turbine vane segment. *Theor. Appl. Fract. Mech.* **86**, 143–152 (2016)
- G. Fischer, B. Tilg, R. Modre, G.J.M. Huiskamp, J. Fetzer, W. Rucker, P. Wach, A bidomain model based BEM–FEM coupling formulation for anisotropic cardiac tissue. *Ann. Biomed. Eng.* **28**, 1229–1243 (2000)
- R.A. Bialecki, Z. Ostrowski, A.J. Kassab, Q. Yin, E. Scuibba, Coupling BEM–FEM and analytic solutions in steady-state potential problems. *Eng. Anal. Bound. Elem.* **26**, 597–611 (2002)
- D. Soares Jr., L. Godinho, Heat conduction analysis by adaptive iterative BEM–FEM coupling procedures. *Eng. Anal. Bound. Elem.* **73**(2016), 79–94 (2016)
- A. Landenberger, A. El-Zafrany, Boundary element analysis of elastic contact problems using gap finite elements. *Comput. Struct.* **71**(1999), 651–661 (1999)

24. L. Rodríguez-Tembleque, R. Abascal, A 3D FEM–BEM rolling contact formulation for unstructured meshes. *Int. J. Solids Struct.* **47**(2010), 330–353 (2010)
25. O. Czygan, O. von Estorff, Fluid-structure interaction by coupling BEM and nonlinear FEM. *Eng. Anal. Bound. Elem.* **26**(2002), 773–779 (2002)
26. G.N. Gatica, A. Márquez, S. Meddahi, Analysis of the coupling of BEM, FEM and mixed-FEM for a two-dimensional fluid–solid interaction problem. *Appl. Numer. Math.* **59**(11), 2735–2750 (2009)
27. O. von Estorff, M. Firuziaan, Coupled BEM/FEM approach for nonlinear soil/structure interaction. *Eng. Anal. Bound. Elem.* **24**(2000), 715–725 (2000)
28. G. Vasilev, S. Parvanova, P. Dineva, F. Wuttke, Soil-structure interaction using BEM–FEM coupling through ANSYS software package. *Soil Dyn. Earthq. Eng.* **70**(2015), 104–117 (2015)
29. G.C. Hsiao, F. Liu, J. Sunb, L. Xu, A coupled BEM and FEM for the interior transmission problem in acoustics. *J. Comput. Appl. Math.* **235**(2011), 5213–5221 (2011)
30. Y.H. Wu, C.Y. Dong, H.S. Yang, A 3D isogeometric FE-IBE coupling method for acoustic-structural interaction problems with complex coupling models. *Ocean Eng.* **218**(2020), 108183 (2020)
31. D.C. Rodopoulos, T.V. Gortsas, S.V. Tsinopoulos, D. Polyzos, Nonlinear BEM/FEM scalar potential formulation for magneto-static analysis in superconducting accelerator magnets. *Eng. Anal. Bound. Elem.* **113**(2020), 259–267 (2020)
32. T. Rübberg, L. Kielhorn, J. Zechner, Electromagnetic devices with moving parts—simulation with FEM/BEM coupling. *Mathematics.* **2021**(9), 1804 (2021). <https://doi.org/10.3390/math9151804>
33. H.S. Yang, C.Y. Dong, Y.H. Wu, Non-conforming interface coupling and symmetric iterative solution in isogeometric FE–BE analysis. *Comput. Methods Appl. Mech. Eng.* **373**(2021), 113561 (2021)
34. J.L. Wearing, M.A. Sheikh, A combined finite element boundary element technique for stress analysis, in *6th International Conference on Boundary Element Technology X*, Vol. 1, ed. by C.A. Brebbia (Computational Mechanics Publications, London, 1988)
35. R. Perera, E. Alarcon, FE-BE coupling methods for elastoplasticity. *Commun. Numer. Methods Eng.* **13**, 785–792 (1997)
36. G. Beer, *Programming the Boundary Element Method*. (Wiley, Chichester, 2001)
37. L.M. Bezerra, J.M.S. Medeiros, F.G. Cesari, P. Battistella, Simple numerical techniques using boundary element method for the determination of KI in fracture mechanics. *Transactions* **16** (2001)
38. P.K. Banerjee, R. Butterfield, *Boundary Element Methods in Engineering Science*, 2nd edn. (McGraw-Hill, London, 1981)
39. D.R.J. Owen, A.J. Fawkes, *Engineering Fracture Mechanics*. (Pineridge Press Ltd, Swansea, 1983)
40. M.F. Light, A.R. Luxmoore, A numerical investigation of post-yield fracture. *J. Strain Anal.* **12**(4), 1977 (1977)
41. A.P. Kfoury, Continuous crack growth or quantized growth steps? *Int. J. Fract.* **15**(1), 23–29 (1979)
42. J.R. Rice, A path-independent integral and the approximate analysis of strain concentration by notches and cracks. *J. Appl. Mech.* **29**, 379–386 (1968)
43. J.R. Rice, G.F. Rosengren, Plane strain deformation near a crack tip in a power-law hardening material. *J. Mech. Phys. Solids.* **16**, 1–13 (1968)
44. J.W. Hutchinson, Singular behaviour at the end of a tensile crack in a hardening material. *J. Mech. Phys. Solids.* **16**, 13–31 (1968)
45. C.C. Lin, E.C. Lawton, J.A. Caliendo, L.R. Anderson, An iterative finite element-boundary element algorithm. *Comput. Struct.* **39**, 899–909 (1996)
46. W.M. Elleithy, M. Tanaka, A. Guzik, Interface relaxation FEM–BEM coupling method for elasto-plastic analysis. *Eng. Anal. Bound. Elem.* **28**(7), 849–857 (2004)
47. D. Soares Jr., Soares an optimised FEM–BEM time-domain iterative coupling algorithm for dynamic analyses. *Comput. Struct.* **86**, 1839–1844 (2008)
48. G. Yagawa, Y. Takahashi, K. Kashima, Elastic-plastic analysis on stable crack growth for center cracked plate: a benchmark study. *Eng. Fract. Mech.* **19**(4), 755–769 (1984)
49. M. Fleming, Y. Chu, B. Moran, T. Belytschko, Enriched element-free Galerkin methods for crack tip fields. *Int. J. Numer. Methods Eng.* **40**, 1484–1504 (1997)
50. M.H. Bleackley, A.R. Luxmoore, Comparison of finite element solutions with analytical and experimental data for elastic–plastic cracked problems. *Int. J. Fract.* **22**, 15–39 (1983)

**Publisher’s Note** Springer Nature remains neutral with regard to jurisdictional claims in published maps and institutional affiliations.